Catalysis Today 423 (2023) 114271

Contents lists available at ScienceDirect

Catalysis Today

journal homepage: www.elsevier.com/locate/cattod

A study of CO_2 hydrogenation over Ni-$MgAlO_x$ catalysts derived from hydrotalcite precursors

Andrea Fasolini [a,b,1], Elena Spennati [c,d,1], Sina Ebrahim Atakoohi [c], Matteo Percivale [c], Guido Busca [c,d,*], Francesco Basile [a,b], Gabriella Garbarino [c,d,*]

[a] Dipartimento di Chimica Industriale "Toso Montanari", Alma Mater Studiorum Università di Bologna, Viale Risorgimento 4, 40136 Bologna, Italy
[b] Center for Chemical Catalysis - C3, Alma Mater Studiorum Università di Bologna, Viale Risorgimento 4, 40136 Bologna, Italy
[c] Università degli Studi di Genova, Dipartimento di Ingegneria Civile, Chimica e Ambientale (DICCA), Laboratorio di chimica delle superfici e catalisi, Via Opera Pia 15, 16146 Genova, Italy
[d] INSTM, Via G. Giusti, 50121 Firenze, Italy

ARTICLE INFO

Keywords:
Hydrotalcite
Nickel catalysts
CO_2 methanation
Reverse water gas shift

ABSTRACT

Ni/Mg/Al mixed oxides have been prepared by decomposing corresponding layered double hydroxides of the hydrotalcite family. XRD, FTIR and UV–vis–NIR analyses show that prepared materials are constituted by a rock-salt type $Mg_{1-x}Ni_xO$ solid solution with Al^{3+} in tetrahedral interstices of the cube close packing of oxide anions. When activated at sufficiently high temperature, they convert into optimal size supported Ni metal catalysts which show very active and selective for CO_2 methanation. Catalytic data show that these materials are more active at low temperature than Ni/γ-Al_2O_3 catalysts, with a comparable enhanced activity with respect to Ni/La_2O_3-Al_2O_3 ones. A role of basic oxides as activating components can be envisaged and related to the strength of the adsorption of CO_2 on the "support" likely forming surface (bi)carbonates as active species. Activation energies and reactions orders have been calculated by flow reactor studies in differential reactor conditions. IR spectroscopy data show that carbon dioxide adsorbs on the reduced catalyst in the form of hydroxycarbonates, that convert at higher temperature in carbonates and strongly adsorbed linear and bridging carbonyl species on metallic nickel. The formation of surface CH_x species is also evident.

1. Introduction

In recent years, the methanation of CO_2 with green hydrogen received much attention being a potential way to reuse carbon dioxide, with a reducing effect on greenhouse gas emissions [1–4]. Even though ruthenium-based catalysts extremely active for this reaction, nickel gained high consideration for its remarkable activity, selectivity robustness, and its natural abundance together with limited costs. Being γ-alumina the most applied support for such catalytic materials, it is however well known that the activity and stability of Ni/γ-Al_2O_3 can be significantly modified by adding additional components, aiming at an improved stability and limited deactivation. As an example, it has been found that the addition of silica to the alumina support successfully stabilizes Al_2O_3, but it decreases the catalytic activity of Ni/SiO_2-γ-Al_2O_3 in CO_2 methanation reaction [5], while lanthanum species addition [6] improves both stability and catalytic performances even in the presence of SiO_2, as alumina modifier [7]. Thus, the modification of support acido-basicity is certainly involved in such phenomena and proper tailoring is an open challenge for optimal catalytic performances. Recent advances in lanthanides modification of Ni-based catalysts have been extensively reviewed [8], together with commercial and pilot plant catalysts.

Thus, to try to further increase low-temperature activity of such catalysts, we tested catalysts also containing magnesia, typically a basic surface component. To produce high-surface-area bivalent/trivalent cations mixed oxides catalytic precursors, hydrotalcite-like layered double hydroxides can be conveniently prepared. This methodology, first described in the scientific literature by J. Ross for the preparation of Ni/Al_2O_3 catalysts [9], allowing to prepare homogeneous series of catalytic precursor materials characterized in a large compositional range

* Corresponding authors at: Università degli Studi di Genova, Dipartimento di Ingegneria Civile, Chimica e Ambientale (DICCA), Laboratorio di chimica delle superfici e catalisi, Via Opera Pia 15, 16146 Genova, Italy
E-mail addresses: Guido.Busca@unige.it (G. Busca), gabriella.garbarino@unige.it (G. Garbarino).
[1] equal contribution

https://doi.org/10.1016/j.cattod.2023.114271
Received 16 March 2023; Received in revised form 8 June 2023; Accepted 16 June 2023
Available online 19 June 2023

of spinel/rock salt $NiO/NiAl_2O_4/Al_2O_3$ solid solutions [10,11], and well characterized Ni/Mg/Al mixed oxide samples [12]. This methodology was later largely developed by Angelo Vaccari and his coworkers [13,14] for the synthesis of many different and complex catalytic systems. Indeed, ex-hydrotalcite Mg-Al oxides constitute surface basic solids [15] which act, as shown by Vaccari et al., as robust and activating supports for many metallic catalysts [16–18].

Ni-Al and Ni-Mg-Al hydrotalcite have been recognized as suitable precursor for CO_2 hydrogenation [19–22] and their possible application has been recently reviewed [23], even though, to best of our knowledge, mechanisms and experimental kinetics are apparently lacking for low Ni-loading Mg hydrotalcite derived catalysts.

In the present work the characterization of Ni- over Mg/Al mixed oxide catalytic materials and their precursors, in relation to their catalytic activity in the CO_2 hydrogenation at atmospheric pressure will be presented, shading light on the effect of prereduction, mechanism and kinetic evaluation.

2. Experimental

Optimized coprecipitation technique was used to synthetize the Ni/Mg/Al layered double hydroxide (LDH) precursors [24,25]. To do so, Ni $(NO_3)_2{\cdot}6\ H_2O$ (99 %, Sigma Aldrich), $Mg(NO_3)_2{\bullet}6\ H_2O$ (99 %, Sigma Aldrich) and $Al(NO_3)_3{\bullet}9\ H_2O$ (99 %, Sigma Aldrich) were dissolved in water (2.0 M) and these solutions were slowly added to the aqueous solutions containing Na_2CO_3 (1.0 M) at 333 K and pH 10. During the addition the pH was kept at 10.0 ± 0.5 by addition of a 3.0 M NaOH aqueous solution. The molar ratio of the Ni, Mg and Al precursors was modified for the two samples as shown in Table 1, while using a constant $Na_2CO_3/Al(NO_3)_3{\bullet}9\ H_2O$ molar ratio equal to 2. The obtained suspensions were stirred for 45 min (at 333 K), and the solids were recovered by filtration and washed with deionized water (washing volume = 2 L). The obtained compounds were dried at 343 K for 18 h, then grinded to yield the LDH powders. Obtained materials were calcined at 923 K for 12 h with a ramp of 10 K/min ramp to yield the corresponding Ni/Mg/Al mixed oxides.

2.1. Characterization of the catalytic materials

Powder X-ray diffraction (XRD) analysis was carried out using a Philips PW1050/81 diffractometer. The instrument had a graphite monochromator in the diffracted beam which was associated with a PW1710 unit (Cu Kα, λ = 0.15418 nm). The analysis was performed at 0.1°/s, in the 2θ range from 5° to 80°.

A Micromeritics ASAP 2020 instrument was used to investigate surface area (derived with BET method), as well as pore volume and diameter. N_2 adsorption-desorption isotherms were determined at 77 K. Before the analysis, the samples were pretreated to eliminate eventual impurities. The sample was heated up at 423 K and 30 mmHg (30 min at this temperature) and finally heated up to 523 K and kept at this temperature for 30 min, in order to eliminate all the impurities that can be absorbed on the surface of the sample.

FT-IR spectra of fresh catalysts and pure supports were collected with a Nexus Thermo Fisher instrument with 100 scans and spectra resolution of 2 cm^{-1}. A pressed disk with 1 wt% of sample KBr to a total weight of 1.00 g was used for skeletal spectra analysis.

Diffuse Reflectance UV–visible-near infrared (DR-UV–vis–NIR) spectra of fresh catalysts were collected with a V570 instrument (JASCO Corp., Tokyo, Japan) equipped with an integrating sphere. The sample has been gently pressed in the sample holder without other treatments.

The reducibility properties of the catalyst were studied using Temperature Programmed Reduction (TPR) in a Micromeritics Autochem II Chemisorption Analyzer equipped with a TCD detector. Before TPR measure, the samples were pre-treated in He (30 mL/min) at 423 K (for 30 min). After cooling the sample to 323 K, the TPR analysis was started by flowing a 5 % (v/v) H_2/Ar mixture (30 mL/min) and increasing the temperature at a rate of 10 K/min from 323 K to 1123 K. Finally, the sample was kept at 1223 K for 30 min, then cooled down under He flow.

The same Micromeritics Autochem II Chemisorption Analyzer instrument was used to investigate the base properties of the samples by CO_2 temperature programmed desorption (TPD). A pretreatment in He at 673 K for 45 min was carried out, then the temperature was decreased to 373 K under He. The sample was firstly saturated with a flux of CO_2 10 % (v/v) in He (30 mL/min for 1 h) and then purged with pure He (30 mL/min) for 1 h to remove physisorbed CO_2. Desorption measurements were performed up to 773 K with a ramp of 10 K/min.

CO adsorption was performed at 140 K by the introduction of a known dose of the gas (6 torr) inside the low temperature infrared cell containing the previously activated wafers, by reduction at 773 K for 1 h and a H_2 pressure of 300 torr. IR spectra were recorded during evacuation upon warming at increasing temperatures between 140 K and 673 K.

2.2. Catalytic experiment

Catalytic experiments were carried out in a tubular fixed-bed silica glass reactor, loaded with 88 mg of catalyst and 700 mg of silica particles (60–70 mesh). 80 NmL/min of gaseous reactant mixture, with H_2/CO_2 ratio of 5 in diluted condition with nitrogen, were fed to the reactor, by keeping a GHSV of 55,000 h^{-1}. The reaction temperature was varied step by step from 523 to 773 K (ascending temperature test) and from 773 to 523 K (descending temperature test) to evaluate a possible catalyst deactivation. The product stream composition was analyzed at each temperature by using a gas chromatograph, model 4890 (Agilent Technologies, Santa Clara, CA, USA), with FID and TCD detectors. The instrument is equipped with a Varian capillary column, model Molsieve 5 A/Porabond Q Tandem (Agilent) and helium (purity > 99.9 %) is used as a carrier gas.

The flow rate of the product was estimated at each temperature step in order to evaluate CO_2 conversion (X_{CO2}), products yield (Y_i, with i = CO, CH_4) and selectivity (S_i, with i = CO, CH_4) ad shown in Eq. (1), Eq. (2), and Eq. (3), respectively.

$$X_{CO2} = \frac{F_{CO2in} - F_{CO2out}}{F_{CO2in}} \quad (1)$$

$$Y_i = \frac{F_i}{F_{CO2in}} \quad (2)$$

$$S_i = \frac{F_i}{F_{CO2in} - F_{CO2out}} \quad (3)$$

In order to evaluate the effect of catalyst pre-reduction temperature, sample A has been reduced in situ under reducing environment (20 % H_2 and 80 % N_2, total flow rate 80 NmL/min) at 773 and 923 K for 3 h with a heating ramp of 25 K/min. Then, sample B has been pre-reduced at the best condition found out for sample A.

Kinetic aspects have been evaluated on the catalyst (88.1 mg of catalyst diluted with 700 mg of silica glass) pre-reduced and tested at the conditions previously reported. The estimation of apparent activation energies, by using Arrhenius plot, was evaluated by performing the CO_2 methanation reaction at 493, 508 and 523 K, where the conversion values are under kinetic control. The evaluation of CO_2 reaction order was performed by varying the CO_2 partial pressure (P_{CO2}) between 0.03 and 0.07 atm and maintaining constant the H_2 one (P_{H2}= 0.30 atm). For the evaluation of H_2 reaction order, its partial pressure (P_{H2}) was varied

Table 1
Molar composition of the LDH precursors.

Catalyst	Ni (mol%)	Mg (mol%)	Al (mol%)	M^{2+}/M^{3+} ratio
A	24	51	25	3
B	24	56	20	4

between 0.03 and 0.28 atm and P_{CO2} was kept constant at (0.07 atm). The experiment has been carried out, under the hypothesis of a differential reactor, at 493 and 523 K to assess variation in obtained reaction orders.

The catalytic reaction has been also performed in static conditions in the IR cell using pressed disks of the pure catalyst powder after previous reduction in hydrogen at 337 torr and 773 K for 1 h. Then, the sample was put in contact with pure H_2 (194 torr) at r.t. (room temperature) and subsequently with additional 47 torr of CO_2. After gas exposure and collection of gas and surface spectra, the reaction temperature was increased step by step with the same procedure previously reported for catalytic experiments. At each tested temperature, IR spectra of the gas phase and of the catalysts were recorded in sequence.

3. Results and discussion

3.1. Characterization of mixed oxide catalyst precursors

XRD analysis was carried out to probe the structure of the as-prepared and calcined samples. The as-prepared samples (Fig. 1) show the characteristic pattern of layered double hydroxides (LDH, hydrotalcite-like), with no other phase detected. The LDH structure is composed by layers of mixed hydroxides in a brucite-like structure, alternated with layers of carbonates anions. The layering is driven by the presence of Al^{3+} whose excess of charge in the brucite-like sheet must be counterbalanced by an anion (carbonate). A slight shift toward lower 2θ is observed by the characteristic peaks at around 11 (003), 23 (006) and 35 2θ (009), when the M^{2+}/M^{3+} ratio is increased. This shift has been also observed when rehydration of Mg-Al hydrotalcite occurred [26].

Calcination of the LDH precursors at 923 K provided the formation of a defective mixed oxide structure, with the rock salt structure of MgO (periclase) and/or NiO (bunsenite), or of their solid solution $Mg_xNi_{1-x}O$, following the collapse of the LDH with the concurrent formation of CO_2 from carbonates decomposition. Reported diffraction pattern well correspond with the one available for $Mg_{0.7}Ni_{0.3}O$ (NaCl, cF8225). In the case of sample A, no other segregated phases were clearly observed indicating that Ni, Mg and Al are mostly interspersed in the mixed oxide. However, the presence of amorphous material cannot be excluded in samples obtained from decomposition of layered double hydroxides and the shoulder at 35° may be related to the presence of amorphous Ni-doped alumina or of an hydroxycarbonate phase as reported by Trifirò et al. [27,28]. Sample A does not show evident features of a spinel structure while they appear in the XRD pattern of sample B, where, together with sharper peaks, very weak components also appear (see asterisks in the figure), which may correspond to peaks of a spinel phase ($MgAl_2O_4$, cF56).

In Fig. 2, the skeletal FT-IR spectra of the two calcined samples are reported. The main peak, a little broader for sample B than for sample A, observed at 410 cm^{-1} is typical of the transverse optical mode of the only IR active mode of the rock salt type, observed near 400 cm^{-1} for both MgO monocrystals [29,30] and NiO monocrystals [31], and usually shifted a little up for the corresponding powdered samples [25,32]. The pronounced shoulder found near 650 cm^{-1} is due to the corresponding longitudinal optical mode [25–27]. Thus, a salt-rock type phase, either MgO or NiO or, more likely, a $Ni_xMg_{1-x}O$ solid solutions, whose formation is likely being associated to negative enthalpies [33], is confirmed. However, the additional evident absorption split at 850, 800 cm^{-1} never is found in the spectra of pure rock salt type oxides. The position of this band is typical of absorptions of aluminate spinels [34], attributed to the vibrations of oxygen bridging between cations in tetrahedral and octahedral sites. In fact, these vibrational modes are observed at higher frequency than the vibrations of oxygens bridging between octahedrally coordinated cations, like they exclusively exist in rock-salt type structures. However, XRD does not reveal significant amounts of spinel phases in investigated samples. Taking into account the strong preference of Ni^{2+} for octahedral coordination for electronic reasons, evident also by the observation that $NiAl_2O_4$ is an inverted

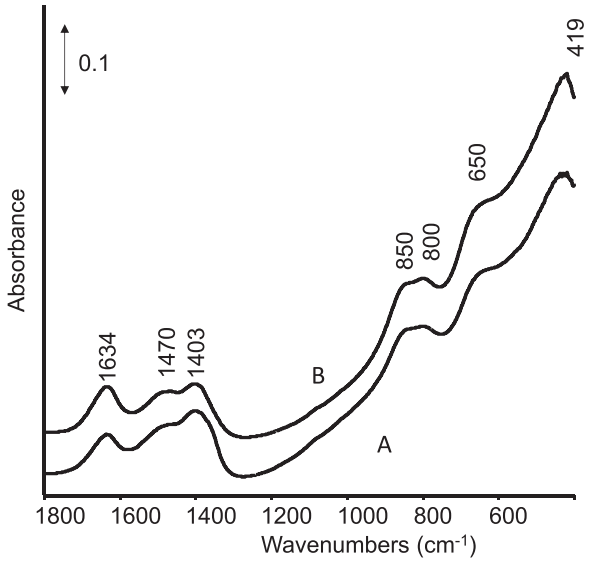

Fig. 2. FT-IR skeletal spectra of A and B catalysts.

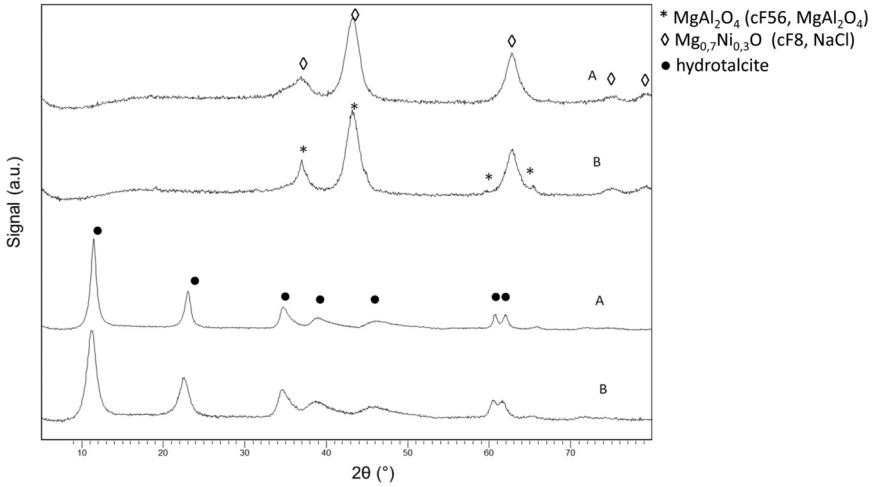

Fig. 1. XRD patterns of the as-prepared NiMgAl layered double hydroxides and mixed oxides.

spinel [35], while $MgAl_2O_4$ is a normal spinel [36] with Mg^{2+} in tetrahedral coordination, the spectrum suggests that either part of Mg^{2+} or at least part of Al^{3+} ions stay in tetrahedral sites in this material. According to previous studies [37–39], these features are very likely associated to Al^{3+} ions in tetrahedral sites likely present as defect sites in the rock-salt type matrix.

IR spectra also show the presence of bands at 1450 and 1403 cm^{-1}, which are due to carbonate ions still trapped in the mixed oxide phase after decomposition of hydrotalcite type hydroxy-carbonate.

In Fig. 3 the UV–vis–NIR spectra of the samples are reported. The strong absorptions, associated to the green hues of investigated samples, are all due to transitions of involving Ni^{2+} ions, considering that neither Mg^{2+} nor Al^{3+} have electrons in d orbitals and that MgO, Al_2O_3 and $MgAl_2O_4$ do not present significant absorptions in the entire range. The spectra are compared with those found for NiO and $NiAl_2O_4$. The strong absorption in the UV region is associated to O^{2-} (2p) → Ni^{2+} (3d) charge transfer transitions: the maximum lies below the cut-off at 250 nm, and this is typical of quite isolated Ni^{2+} ions. The other absorptions are all due to d–d transitions of octahedrally coordinated Ni^{2+} [40]. In particular, the absorption near 400 nm is associated to the $^3A_{2\,g}$ → $b^3T_{1\,g}$, the doublet in the visible region is attributed to the $^3A_{2\,g}$ → $a^3T_{1\,g}$ and the $^3A_{2\,g}$→ a^1E_g while that in the near infrared region is attributed to the $^3A_{2\,g}$ → $a^3T_{2\,g}$. However, the shape and position of these absorptions are clearly different from those of NiO as well as of $NiAl_2O_4$, reported as well in Fig. 3. Thus, the data, in good agreement with neutron diffraction data previously reported for similar samples [29], show that the materials are constituted by a rock-salt type $Mg_{1-x}Ni_xO$ solid solution with Al^{3+} ions in tetrahedral interstices and, necessarily, octahedral sites vacancies, and additional residual carbonate species trapped on pores.

In Table 2 the morphological properties of the samples, as analysed by nitrogen physisorption, are summarized. Higher surface area is observed for the sample A, with lower Al content, in fact, part of the developed surface area is caused by the decomposition of carbonates to gaseous carbon dioxide during calcination, and a low Al content, entails a decreased carbonates amount, which intercalates to counterbalance the Al charge. This is also true for pore volume and diameter values that are found to be higher for sample A than sample B, in line with a high Al content. Indeed, while the structural properties of the two samples are very similar, they significantly differ for morphological properties, with a high surface areas and porosity for sample A, associated to a lower crystallinity as apparently evidenced by XRD.

The analysis of the isothermal linear plots provides a deeper analysis of the catalyst morphology (Fig. 4). Both samples can be classified as mesoporous as depicted by the type IV isotherms. [41]. The higher isotherm of sample A is caused by to the presence of many pores and a high pore volume, that results in high gas adsorption by capillary condensation at high relative pressures. Different hysteresis are displayed by the two samples. Sample A is characterized by a type H1 hysteresis that is peculiar of pores with uniform size and shape. On the other hand, sample B shows a type H2 hysteresis indicative of ink-bottle pores. Thus, the different amount of Al in the sample, not only influences the surface area and pore volume but also the pore shape. In facts, high Al content, i.e., high amount of carbonates in the catalyst precursor, allows the creation of uniform pores during its decomposition to oxide. In contrast, when a diminished number of carbonates modifies the carbon dioxide evolution throughout the material leading to the formation of ununiform pores.

The redox properties of the catalysts were investigated by Temperature Programmed Reduction (TPR, Fig. 5). The two catalytic systems were characterized by a broad reduction peak. Sample A showed a reduction at slightly lower temperatures, starting at 923 K and having a maximum at 1123 K, compared to Sample B (943 and 1173 K). As the Ni^{2+} that is reduced to its metallic form during the TPR analysis is originally in large part inside the structure of the mixed oxide, the better reducibility of the sample with higher Al content, is ascribed to its higher surface area. Having a look at the hydrogen consumption, the two samples showed a similar incomplete overall Ni reduction (79 % and 83 %) indicating that most of Ni^{2+} has been reduced, though a part of it is not accessible being trapped in the bulk of the mixed oxide.

Table 2
BET surface area (m^2/g), pore volume and diameters of the calcined catalysts.

Sample	BET surface area (m^2/g)	Pore volume (cm^3/g)	Pore diameter (nm)
A	173	0.73	11.8
B	135	0.31	7.1

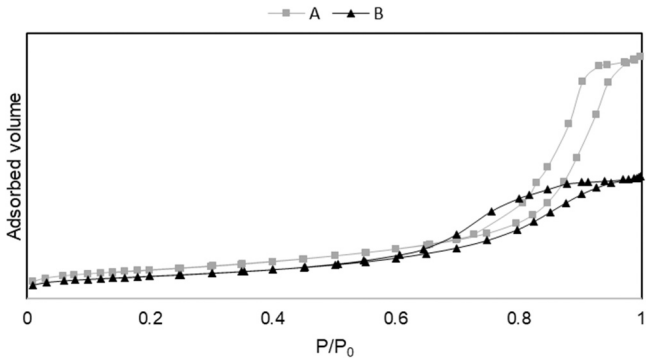

Fig. 4. Isothermal linear plots of nitrogen adsorption at 77 K on samples A and B.

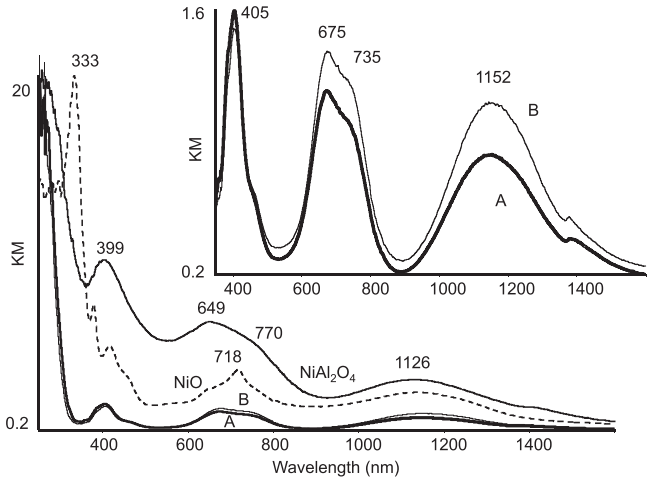

Fig. 3. UV–vis–NIR spectra of A and B catalyst compared with these of NiO and $NiAl_2O_4$ powders.

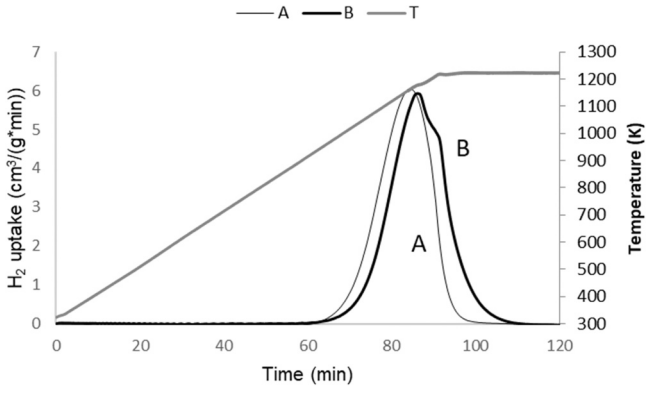

Fig. 5. Temperature Programmed Reduction (TPR) curves of the investigated catalysts.

CO_2 Temperature Programmed Desorption analysis (TPD) was used to investigate strength of catalyst base sites (Fig. 6). They show one broad desorption peak below 773 K that indicates the presence of weak-medium basic sites. Desorption temperatures higher than 773 K were not investigated as at high temperatures, the mixed oxide could modify its phase transforming into MgO and spinel. Quantification of the desorbed CO_2 gives an insight on the sample basicity and the results are shown in Table 3. Sample B showed a higher basicity that is consistent with the higher amount of Mg of this sample. This is further confirmed by normalizing the base site density over the surface area of the sample. In this case, the difference in basicity is even higher for Sample B than A, showing the effect of the variation of the concentration of Mg.

In Fig. 7, low temperature CO adsorption on activated sample A is reported. After activation, carbonate species are still present with a quite complex feature in the range 1700–1300 cm^{-1}, and hydroxy groups as well (see below). A first band near 2160 cm^{-1} with a shoulder at 2153 cm^{-1} is observed before outgassing at very low temperature, thus being assigned to CO interacting with surface ions and CO interacting with surface hydroxyl groups [42]. Upon outgassing a main band at 2163 cm^{-1} and shifting upon temperature increase to 2173 cm^{-1} (223 K) and finally observed at 2169 cm^{-1}, characteristic of CO interaction surface ions and, in particular, suggesting the exposure of Mg at the surface, forming a characteristic Mg-CO unstable carbonyl complex [43]. Even though very weak, a feature at 2079 cm^{-1} is observed and it is assignable to CO adsorbed on-top in terminal coordination; upon outgassing and temperature increase features at 2130, 2060 and 2039 cm^{-1} appear, suggesting also the presence of $Ni(CO)_4$, typical of polycarbonyl species. It has to be pointed out that also a weak feature at 1986 cm^{-1} could be envisage suggesting the presence of bridging species, characteristic of metallic particles [44–46]. The results are in line with data obtained over Ni-Mg/Al_2O_3 catalysts [47], suggesting some surface reconstruction and confirming Mg behavior in increasing the metal particle sizes, as reported by Jensen [48].

3.2. Catalytic results in CO_2 hydrogenation

In Fig. 8, the results of catalytic experiments in CO_2 hydrogenation performed on sample A are reported and compared with forecasted thermodynamic equilibrium data, after two adopted prereduction temperatures i.e., 773 and 923 K. Conversion of CO_2 strongly depends on the pre-treatment temperature. The conversion on sample A, pre-treated at 773 K, is zero at 523 K and increases with temperature and progressively approaching the thermodynamics equilibrium at 723 K. Both CO and CH_4 are produced at low temperature with selectivity to methane approaching 100 % at 673 K and 723 K, in good agreement with the literature [19–22]. Interestingly, the performances during the decreasing temperature experiment are slightly improved below 673 K with respect to those assessed in the increasing temperature experiment, suggesting that the catalyst is essentially stable in this 8 h long experiment, undergoing a slight activation in line with the exothermic behavior of methanation reaction and mild prereduction conditions applied. After prereduction at 923 K, the catalyst is far more active in the 473–723 K temperature range, and also very selective to methane (S_{CH4} ~ 100 % up to 673 K). Equilibrium conversion and selectivities are essentially approached staring from 623 K and above. Also in this case, the catalyst appears to be stable in the full experiment, including both increasing and decreasing temperature steps. The catalyst appears to be more active than some of the catalysts previously tested with similar Ni loadings, as shown in Table 4, even though performances are mostly comparable with promoted Ni-La/Al_2O_3 catalysts [6].

In Fig. 9, the performances of A and B catalysts are compared, both

Table 3
Ni reduction and base sites quantification of the investigated samples.

Sample	Ni^{2+}% reduced in TPR	Base sites from TPD (mL CO_2/g)	Base sites from TPD Norm. on Surface area (mL CO_2/m^2)
A	79%	1.33	0.0077
B	83%	1.58	0.0117

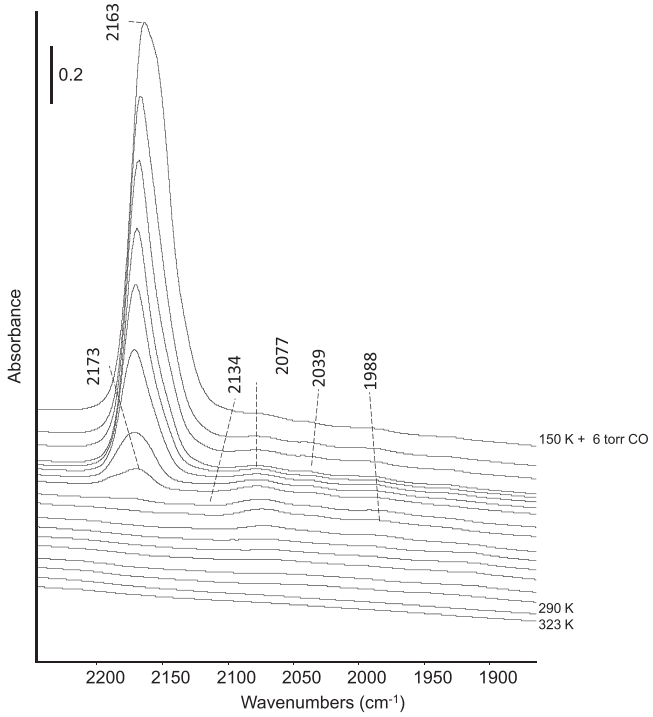

Fig. 7. IR spectra of CO adsorbed at 150 K on A sample (pure powder pressed disks). The uppest spectrum has been recorded in the presence of CO at 150 K, the others upon increasing temperature under outgassing from 150 K to 323 K.

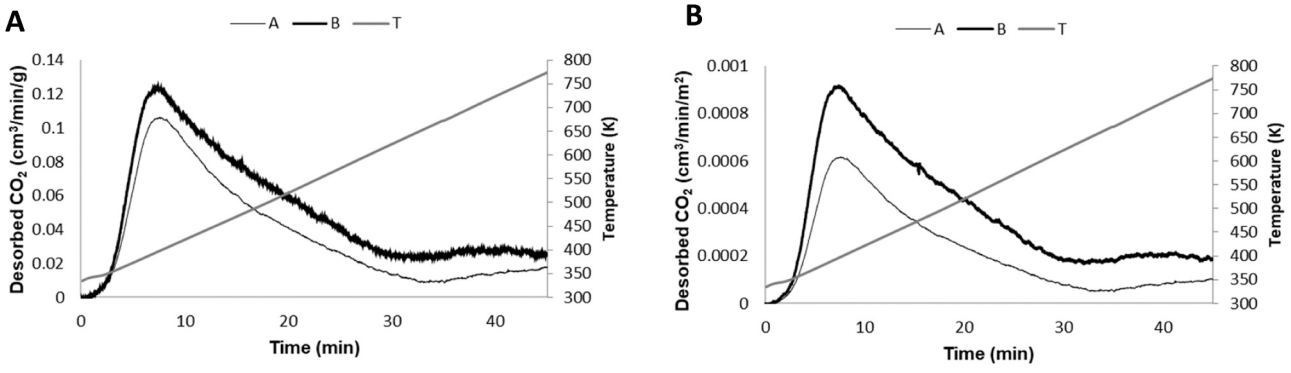

Fig. 6. CO_2 temperature programmed desorption curves of the investigated samples: (A) normalized on sample mass; (B) normalized on surface area.

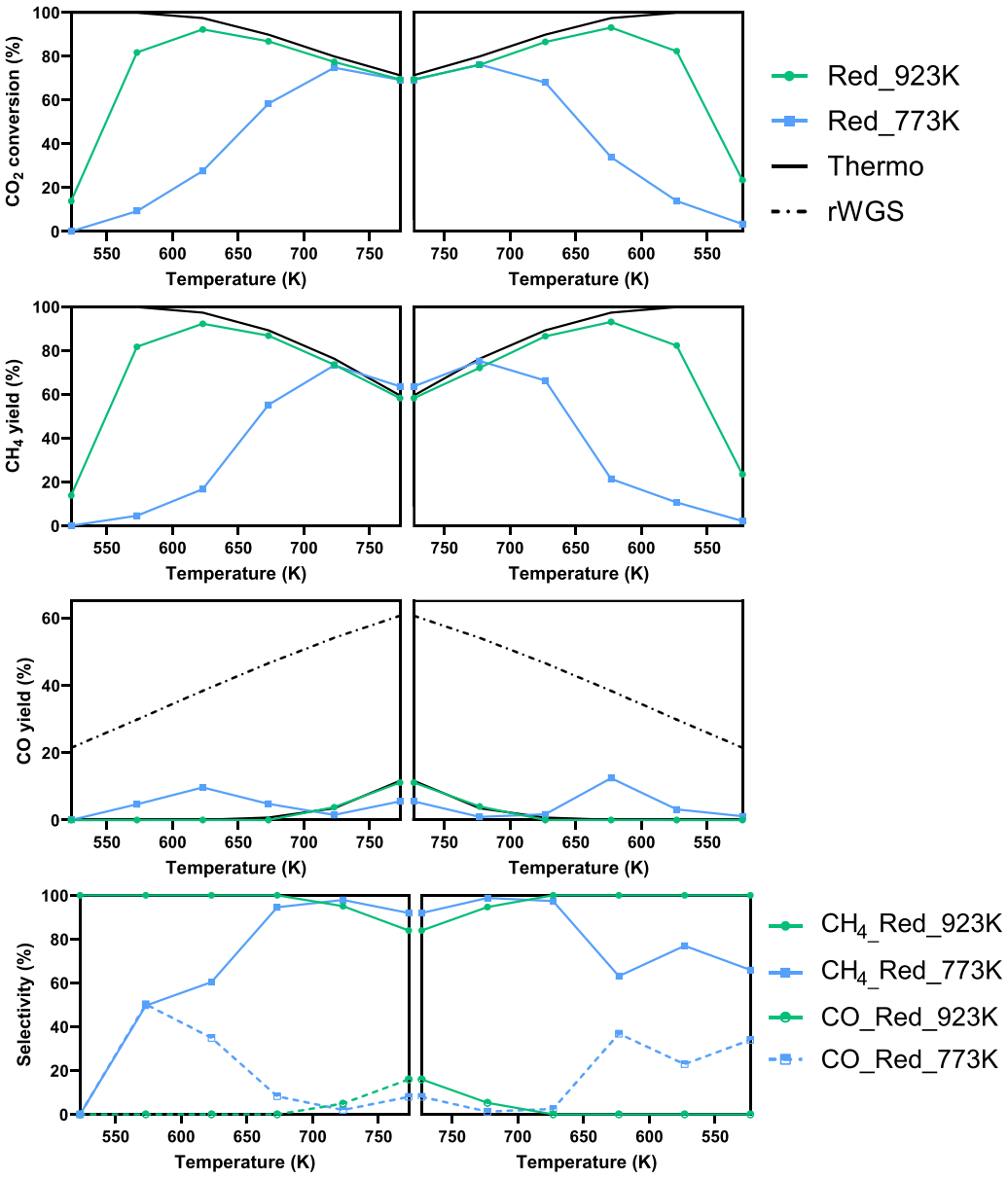

Fig. 8. CO_2 conversion and CH_4 and CO yields and selectivities obtained with A catalyst, reduced at 923 and 773 K, in the temperature range 523–773 K. Data are compered with forecasted thermodynamic equilibria (METH+rWGS - Thermo) and (rWGS).

Table 4
Comparison of CH_4 yield and selectivity obtained at 623 K with literature data.

Sample	Ni loading (wt %)	Y_{CH4} (%)	S_{CH4} (%)	Ref.
A	27.0	92	100	This work
B	27.0	94	100	This work
Ni/Al_2O_3[a]	20.0	54	93	[49]
Ni/SiO_2	26.2	44	89	[5]
Ni/(1 wt.) SiO_2-Al_2O_3	26.2	74	100	[5]
Ni/(20 wt%) SiO_2-Al_2O_3	26.2	48	96	[5]
Ni-La(14 wt%)/Al_2O_3	13.6	92	100	[6]
57–4Q	18	74	98.5	[49]

[a] Catalyst tested without in situ pretreatment

after reduction at 923 K. The behaviors are very similar, within experimental error. In both cases equilibrium conversion and selectivities are essentially approached in the 623–773 K range. Interestingly, after prereduction at 923 K, catalytic performance are stable an no evidenced activation effect is observable.

3.3. Evaluation of kinetic parameters

The kinetic study has been conducted assuming differential reactor hypothesis. In Table 5, the CH_4 production rates, as a function of reaction temperature, are reported for the two catalysts, after prereduction at 923 K, in the 493–523 K temperature range.

In Table 6, the kinetic parameters i.e., reaction orders and activation energies, obtained as evaluated from experiments, are reported and compared with those obtained over other Ni catalysts. From these data, it is evident that at very low temperature and conversion catalyst B is a little more active than catalyst A, being characterized by a lower apparent activation energy (Fig. 10). Lower active activation energy might be associated to higher MgO content. The obtained E_a values are

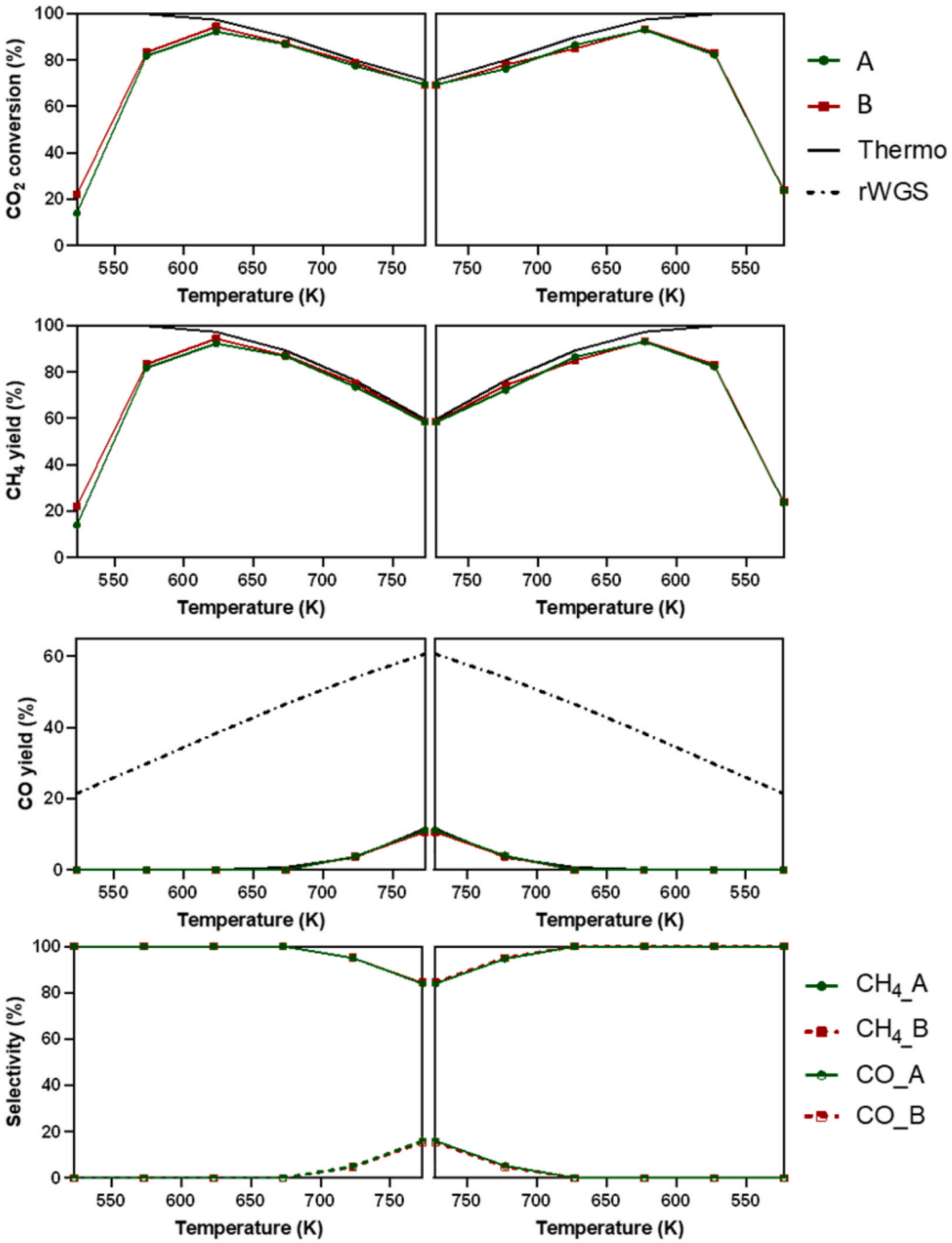

Fig. 9. CO_2 conversion and CH_4 and CO yields and selectivities obtained with A and B catalysts, reduced at 923 K, in the temperature range 523–773 K Data are compered with forecasted thermodynamic equilibria (METH+rWGS – Thermo) and (rWGS).

Table 5
Methane formation rates and yields obtained on A and B catalysts. Reaction conditions: 88.1 mg catalyst, T = 493–523 K, total flow rate 80 NmL/min and H_2:CO_2 = 5:1.

Sample	T (K)	r_{CH4} (mol/min·g)	F_{CH4} (mol/min)	Y_{CH4} (%)
A	493	1,27E-04	1.118E-05	5.2
	508	2,91E-04	2.564E-05	12.0
	523	5,36E-04	4.727E-05	22.0
B	493	1,73E-04	1.522E-05	7.1
	508	3,38E-04	2.980E-05	13.9
	523	5,35E-04	4.712E-05	22.0

Table 6
Apparent reaction orders and activation energies for investigated catalysts and comparison with Ni/Al_2O_3 catalysts.

Sample	Ni content (wt %)	Ea[a] [kJ/mol]	T [K]	α	β	Ref
A	27	103	493	0.03	0.41	This
			523	-	0.55	work
B	27	81	493	0.13	0.37	This
			523	-	0.65	work
Ni/Al_2O_3	20	83	523	0.16	0.32	[54]
Ni/Al_2O_3	13.6	73	523	0.20	0.40	[6]

[a] Ea is apparent activation energy.

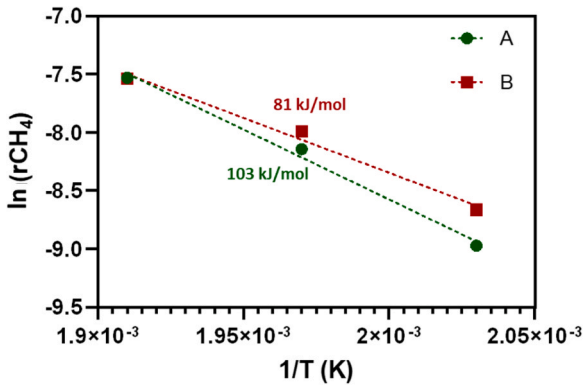

Fig. 10. Arrhenius plot for investigated catalysts and obtained apparent activation energies in CO_2 hydrogenation reaction.

in good agreement with literature data, as shown in Table 6 and as reported for $NiAl(O)_x$ [48] and Ni/Al_2O_3 [49,50], being in all cases higher than values (42–56 kJ/mol) reported for Ni-Al ex-hydrotalcite systems [51].

The reaction orders have been evaluated by using a simple power law model (Eq. 4). In Fig. 11, methane reaction rate as a function of CO_2 and H_2 partial pressures and at different reaction temperature are reported. Validation of achieved data was carried out by fitting methane production rate with a more exhaustive power law equation (Eq. 5):

$$r_{CH4} = k \quad P_{CO2}^{\alpha} \quad P_{H2}^{\beta} \tag{4}$$

$$r_{CH4} = k \quad P_{CO2}^{\alpha} \quad P_{H2}^{\beta}\left(1 - \frac{P_{CH4} \quad P_{H2O}^{2}}{P_{CO2} P_{H2}^{4} \quad K_{eq}}\right) \tag{5}$$

The equilibrium constant (K_{eq}) was estimated with the following empirical formula as reported by Aparicio [52] and used by Koschany et al. [53]:

$$K_{eq} = 137 \bullet T^{-3.998} \exp\left(\frac{158.7 kJ/mol}{RT}\right) \tag{6}$$

The investigated samples presented slightly different reaction orders for both H_2 and CO_2, as shown in Table 6 and Fig. 11. By an increase of the reaction temperature, an increase of H_2 reaction order was observed for both samples, in agreement with what was observed in the case of $NiAl(O)_x$ [48] and Ni/SiO_2 catalysts [55], in the range 0.30–0.55 and with CO_2 reaction orders in the range (0.24–0.07 upon temperature increase). It was suggested the changes in reaction orders with reaction temperature might be related to the presence of different amounts of product gases [48].

The parity plots of the predicted and obtained methane production rates are shown in Fig. 12 for A and B samples at 493 K. The estimated methane rates are in line with that one obtained at all the investigated conditions.

3.4. A study of CO_2 hydrogenation by IR spectroscopy

In Fig. 13, the gas-phase spectra recorded during the CO_2 hydrogenation experiments are reported. Taking into account that H_2 gas is IR undetectable, the spectrum recorded in the presence of the catalyst at room temperature and at 523 K do not show other absorption except those of CO_2 and, in particular, the rotovibrational mode centered at 2340 cm^{-1}. At 573 K the absorptions of both methane (in Fig. 13 the rotovibrational asymmetric stretching mode is evident centered at 3016 cm^{-1}) and the rotovibrational CO stretching mode of CO is also observed very weak at 2140 cm^{-1}. The bands of both CH_4 and CO increase in intensity by increasing temperature. No other compounds are observed. As shown in Table 7, the evaluation of the intensity of the bands using calibration data show that methane selectivity is extremely high, > 99 % in these conditions.

As usual, the spectrum of the catalyst disk (down spectrum in Fig. 14) shows a cut-off limit near 1000 cm^{-1}: below this frequency, bulk metal oxygen stretching fully absorb the radiation. After reduction and outgassing, the spectrum of the catalyst disk shows a quite strong band at 3725 cm^{-1}, due to surface hydroxy groups, and a broad absorption centered around 3500 cm^{-1}, due to residual H-bonded hydroxyls. Additionally, a complex absorption band is present in the range 1700–1300 cm^{-1} due to residual carbonate ions probably trapped in the bulk of the ex-hydrotalcite material.

After contact at room temperature with the CO_2: H_2 1:5 gas mixture, the spectrum is modified with the formation of bands at 3620, 1671, 1415, 1225 cm^{-1} (more evident in the subtraction spectrum in Fig. 15), which are typical of surface monohydrogencarbonate ions (OH stretching, CO_3^{2-} asymmetric and symmetric stretching and OH bending, respectively).

By increasing temperature, a new band forms at 1604 cm^{-1}, which can be due to adsorbed water formed by the methanation reaction, while at even higher temperatures a band at 1544 cm^{-1}, which, together with a further component at 1400 cm^{-1} can be due to a bidentate or polydentate carbonate species.

While linear CO_2 is present with a very weak peak at 2344 cm^{-1} (insert in Fig. 16), with a shoulder at higher frequency, the formation of surface carbonyl species is evident during reaction in the temperature range 523–773 K. In this temperature range, terminal carbonyls are evident in the IR spectra (Fig. 16) at 2063–2057 cm^{-1}, and bridging carbonyls are observed, absorbing at 1910 cm^{-1} after contact at 523 K, and shifted at 1940 cm^{-1} at higher temperature. The former band,

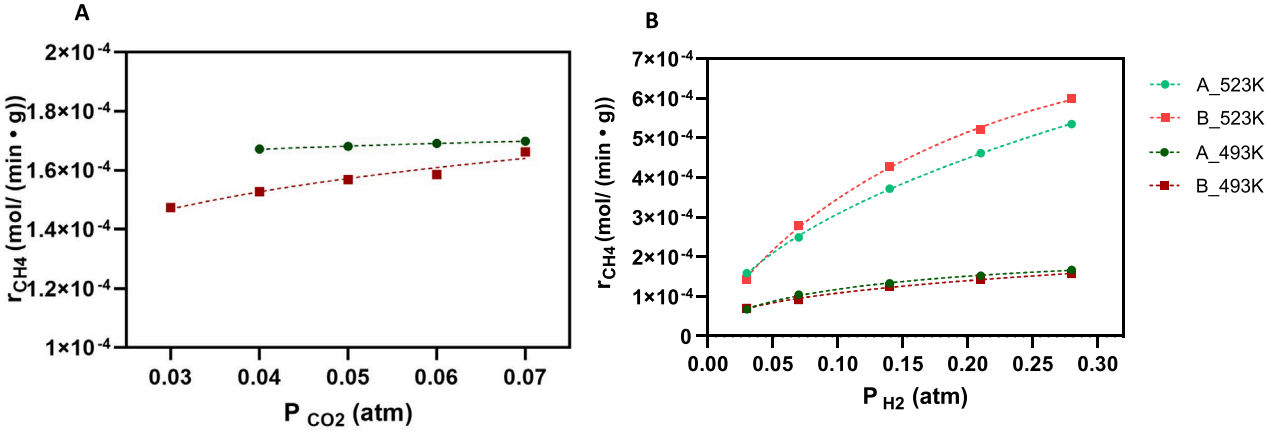

Fig. 11. Experimental evaluation of CO_2 orders for methane production as a function of CO_2 (left) and H_2 (right) partial pressures, respectively.

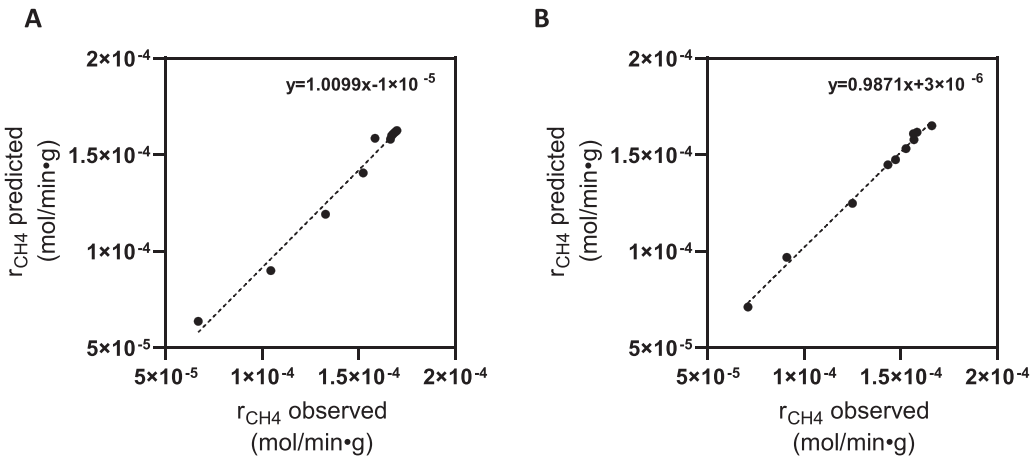

Fig. 12. Parity plot of methane production rates obtained and predicted with sample A (left) and B (right).

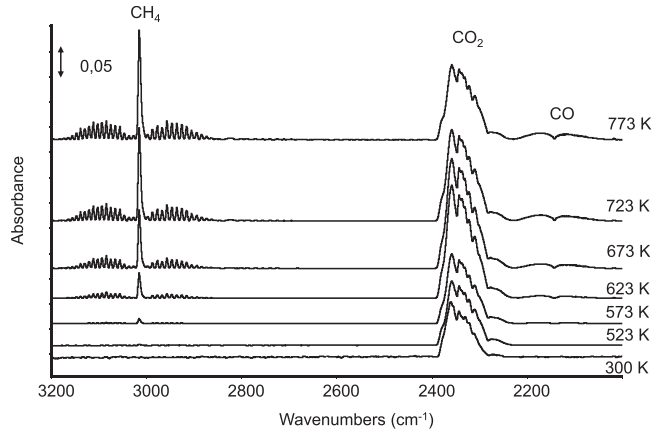

Fig. 13. Gas-phase spectra recorded during the CO_2 hydrogenation in IR cell.

Table 7
CO and CH_4 concentration obtained in CO_2 hydrogenation by IR spectroscopy in the temperature range 523–773 K.

T (K)	C_{CO} (mol/mL)	C_{CH4} (mol/mL)
523	0.000E+ 00	5.674E-07
573	5.087E-09	3.972E-06
623	2.035E-08	1.418E-05
673	3561E-08	3.234E-05
723	4.578E-08	4.936E-05
773	5.087E-08	5.730E-05

typical of terminal nickel carbonyls, shows its maximum slightly shifting from 2063 cm^{-1}, when the band is strongest suggesting that occupation of the face is higher, down to 2057 cm^{-1} when the band is weaker, suggesting a lower CO coverage. The behavior is like that described for CO adsorbed on top on Ni (100) monocrystal faces using different techniques [56,57]. The position of the additional band at 1940–1910 cm^{-1} is typical of the CO stretching of bridging carbonyls observed on different Ni monocrystal faces [41,51,58]. A weak band at 2854 cm^{-1} is also observed, due to a surface CH_x stretching mode. The spectrum in this region does not closely correspond to the CH stretching of formate ions nor of methoxy groups previously observed upon CO hydrogenation on Ni/γ-Al_2O_3 [41] nor to those detected for methoxy and formate groups on MgO-Al_2O_3 oxides [59]. A possible assignment is to a CH_x group on nickel, which is a possible intermediate in the reverse reaction i.e., methane steam reforming on nickel.

4. Discussion

The data reported in this study confirm that hydrotalcite-type Ni,Mg-Al layered double hydroxides allow the production of homogeneous mixed oxides constituted by a rock-salt type $Mg_{1-x}Ni_xO$ solid solution with Al^{3+} in tetrahedral interstices of the cube close packing of oxide anions. The materials, when activated at sufficiently high temperature, convert into supported Ni metal catalysts which are very active and selective for CO_2 methanation. In fact, high temperature is needed for extracting high amounts of Ni from the bulk of the mixed oxide precursor and reducing it. The larger Mg:Al metal ratio in catalyst B allows higher surface basicity resulting in higher CO_2 adsorption ability, and in a slightly higher Ni reduction temperature, also associated to a lower surface area. The catalyst with more magnesium is slightly more active at low temperature, and shows a slightly lower activation energy for methanation. However, it presents a slightly higher reaction order for CO_2 conversion (0.13).

Catalytic data show that these materials are definitely more active at low temperature than Ni/γ-Al_2O_3 catalysts, with a comparable good activity with respect to Ni/La_2O_3-Al_2O_3 ones. A role of base oxides as activating components can be envisaged, and related to the strength of the adsorption of CO_2 on the "support".

IR spectroscopy data show that carbon dioxide adsorbs on the reduced catalyst in the form of hydroxycarbonates, that convert at higher temperature on the working catalyst in carbonates and strongly adsorbed linear and bridging carbonyl species on metallic nickel. The formation of surface CH_x species, possible surface intermediates in methanation, is also evident.

The reported data can be interpreted assuming that the reduction of aluminum-stabilized NiO-MgO based bulk mixed oxide allows to produce optimal-size nickel metal particles which have high hydrogenation activity with limited formation of carbon residues. Otherwise, the optimal basicity of the MgO-Al_2O_3 based support allows medium-strong adsorption of CO_2 which allows its selective full hydrogenation to methane.

5. Conclusions

The high activity and selectivity of Ni catalysts obtained by NiO-MgO-Al_2O_3 mixed oxides derived from hydrotalcite -like precursors in CO_2 methanation has been confirmed. The likely role of surface (bi) carbonate species as active adsorbed CO_2 species is suggested, evidencing the role of an optimal medium basicity of the surface for CO_2 activation. The additional role of the bulk mixed oxide to produce by mild reduction optimal size Ni particles is also underlined. Evidence for the formation of surface CH_x species was provided. Kinetic parameters

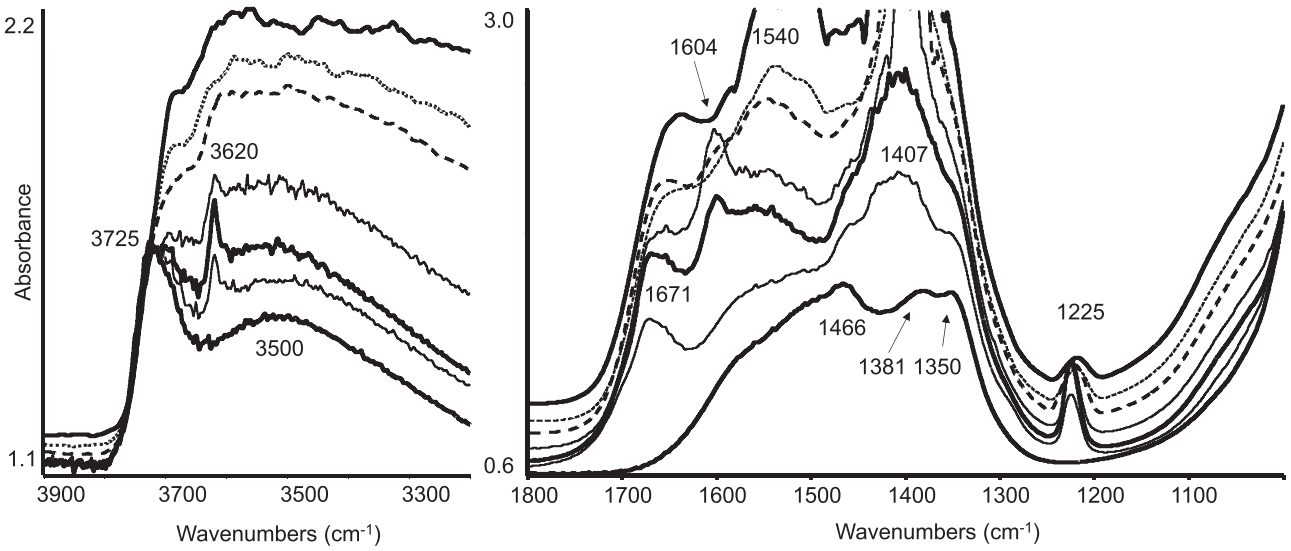

Fig. 14. surface spectra of sample A in the CO_2 hydrogenation reaction carried out in IR cell in the temperature range 523–773 K.

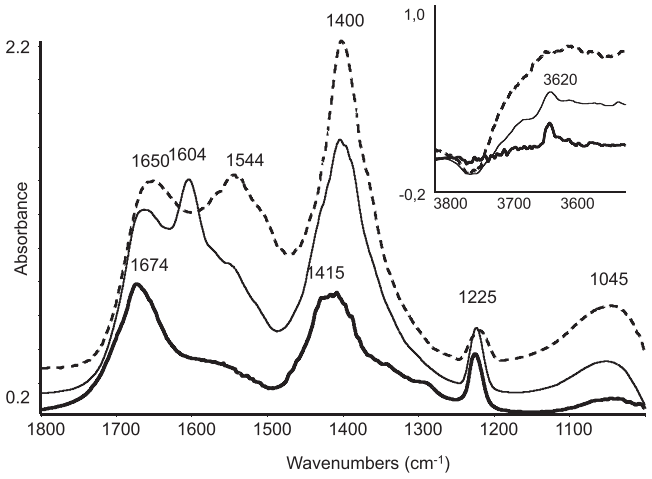

Fig. 15. subtraction spectra of sample A in the CO_2 hydrogenation reaction carried out in IR cell in the temperature range 523–773 K.

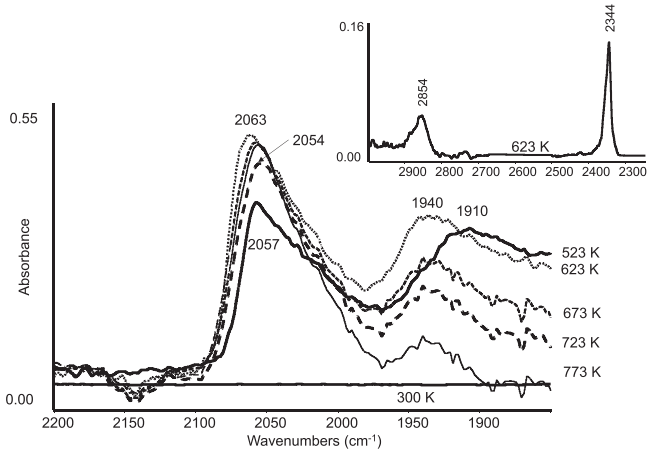

Fig. 16. Subtration of sample A pressed disk and reaction gas in the CO_2 hydrogenation reaction in IR cell in the temperature range 523–773 K.

for the CO_2 methanation reaction were also evaluated.

CRediT authorship contribution statement

Andrea Fasolini experimental work in catalysts preparation and characterization, conceptualization, final revision. **Elena Spennati**: experimental work in catalysts characterization and testing, conceptualization. **Sina Ebrahim Atakoohi**, experimental work in catalysts testing. **Matteo Percivale**, experimental work in catalysts testing. **Guido Busca**: conceptualization, writing draft, final revision. **Francesco Basile**, conceptualization, final revision. **Gabriella Garbarino**: experimental work in catalysts characterization and testing, conceptualization, final revision.

Declaration of Competing Interest

The authors declare that they have no known competing financial interests or personal relationships that could have appeared to influence the work reported in this paper.

Data availability

Data will be made available on request.

Acknowledgments

GG and FB acknowledge funding from European Commission, NextGenerationEU – Piano Nazionale di Ripresa e Resilienza (PNRR) - Ministero dell'Università e della Ricerca (MUR); (project number PE_00000021).

AF aknowledges a research contract co-funded by European Union - PON Ricerca e Innovazione 2014-2020, art. 24, comma 3, lett. a), Legge 30 dicembre 2010, n. 240 e s.m.i. e del D.M. 10 agosto 2021 n. 1062.

References

[1] W. Wang, J. Gong, Methanation of carbon dioxide: an overview, Front. Chem. Sci. Eng. 5 (2011) 2–10.
[2] G. Centi, S. Perathoner, Opportunities and prospects in the chemical recycling of carbon dioxide to fuels, Catal. Today 148 (2009) 191–205.
[3] W. Li, H. Wang, X. Jiang, J. Zhu, Z. Liu, X. Guo, C. Song, A short review of recent advances in CO_2 hydrogenation to hydrocarbons over heterogeneous catalysts, RSC Adv. 8 (2018) 7651–7669.
[4] A. Waldvogel, A. Fasolini, F. Basile, S. Thomas, A.-C. Roger, Effect of the support synthetic method on the activity of Ni/CeZrPr mixed oxide in the Co-methanation

of CO_2/CO mixtures for application in power-to-gas with co-electrolysis, Energy Fuels 35 (2021) 13304–13314.
[5] P. Riani, E. Spennati, M.V. Garcia, V. Sanchez Escribano, G. Busca, G. Garbarino, Ni/Al_2O_3 catalysts for CO_2 methanation: effect of silica and nickel loading, Int. J. Hydr. En. In press, available on internet.
[6] G. Garbarino, C. Wang, T. Cavattoni, E. Finocchio, P. Riani, M. Flytzani-Stephanopoulos, G. Busca, A studu of Ni/La-Al_2O_3 catalysts: a competitive system for CO_2 methanation, Appl. Catal. B: Environ. 248 (2019) 286–297.
[7] P. Riani, I. Valsamakis, T. Cavattoni, V. Sanchez Escribano, G. Busca, G. Garbarino, Ni/SiO_2-Al_2O_3 catalysts for CO_2 methanation: effect of La_2O_3 addition, Appl. Catal. B: Environ. 284 (2021), 119697.
[8] E. Spennati, P. Riani, G. Garbarino, A perspective of lanthanide promoted Ni-catalysts for CO_2 hydrogenation to methane: catalytic activity and open challenges, Catal. Today (2023) (accepted).
[9] E.C. Kruissink, L.L. Van Reijen, J.R.H. Ross, Coprecipitated nickel-alumina catalysts for methanation at high temperature. Part 1. - chemical composition and structure of the precipitates, J. Chem. Soc., Faraday Trans. 1 (77) (1981) 649–663.
[10] O. Clause, B. Rebours, E. Merlen, F. Trifiró, A. Vaccari, Preparation and characterization of nickel-aluminum mixed oxides obtained by thermal decomposition of hydrotalcite-type precursors, J. Catal. 133 (1992) 231–246.
[11] G. Busca, V. Lorenzelli, V. Sanchez Escribano, Preparation, solid-state characterization, and surface chemistry of high surface area $Ni_xAl_{2-2x}O_{3-2x}$ mixed oxides, Chem. Mater. 4 (1992) 595–605.
[12] F. Trifirò, A. Vaccari, O. Clause, Nature and properties of nickel-containing mixed oxides obtained from hydrotalcite-type anionic clays, Catal. Today 21 (1994) 185–195.
[13] P. Gherardi, O. Ruggeri, F. Trifiro, A. Vaccari, G. Del Piero, G. Manara, B. Notari, Preparation of Cu-Zn-Al mixed hydroxycarbonates precursors of catalysts for the synthesis of methanol at low pressure, Stud. Surf. Sci. Catal. 16C (1983) 723–733.
[14] F. Cavani, F. Trifirò, A. Vaccari, Hydrotalcite-type anionic clays: preparation, properties and applications, Catal. Today 11 (1991) 173–301.
[15] D.P. Debecker, E.M. Gaigneaux, G. Busca, Exploring, tuning, and exploiting the basicity of hydrotalcites for applications in heterogeneous catalysis, Chem. - A Eur. J. 15 (2009) 3920–3935.
[16] M. Trombetta, G. Ramis, G. Busca, B. Montanari, A. Vaccari, Ammonia adsorption and oxidation on Cu/Mg/Al mixed oxide catalysts prepared via hydrotalcite-type precursors, Langmuir 13 (1997) 4628–4637.
[17] S. Albertazzi, G. Busca, E. Finocchio, R. Glöckler, A. Vaccari, New Pd/Pt on Mg/Al basic mixed oxides for the hydrogenation and hydrogenolysis of naphthalene, J. Catal. 223 (2004) 372–381.
[18] A. Fasolini, S. Abate, D. Barbera, G. Centi, F. Basile, Pure H2 production by methane oxy-reforming over Rh-Mg-Al hydrotalcite-derived catalysts coupled with a Pd membrane, Appl. Catal. A: Gen. 581 (2019) 91–102.
[19] S. Abate, K. Barbera, E. Giglio, F. Deorsola, S. Bersaid, S. Parathoner, R. Pirone, G. Centi, Synthesis, characterization, and activity pattern of Ni−Al hydrotalcite catalysts in CO_2 methanation, Ind. Eng. Chem. Res. 55 (2016) 8299–8308.
[20] B.C. Kwon, No-K. Park, M. Kang, D. Kang, M.W. Seo, D. Lee, S.G. Jeon, Ho-J. Ryu, CO_2 hydrogenation activity of Ni-Mg-Al_2O_3 catalysts: reaction behavior on $NiAl_2O_4$ and $MgAl_2O_4$, Korean J. Chem. Eng. 38 (2021) 1188–1196.
[21] P. Summa, B. Samojeden, M. Motak, D. Wierzbicki, I. Alxneit, K. Swierczek, P. Da Costa, Investigation of Cu promotion effect on hydrotalcite-based nickel catalyst for CO_2 methanation, Catal. Today 384-386 (2022) 133–145.
[22] A. Müller, P. Völs, B. Störr, F. Mertens, Comparative study of the CO_2 methanation activity of hydrotalcite-based nickel catalysts generated by using different reduction protocols, Catal. Lett. 153 (2023) 1057–1067.
[23] H. Lan Huynh, Z. Yu, CO_2 methanation on hydrotalcite-derived catalysts and structured reactors: a review, Energy Technol. 8 (2020), 1901475.
[24] F. Basile, G. Fornasari, E. Poluzzi, A. Vaccari, Catalytic partial oxidation and CO_2-reforming on Rh- and Ni-based catalysts obtained from hydrotalcite-type precursors, Appl. Clay Sci. 13 (1998) 329–345.
[25] S. Albertazzi, F. Basile, P. Benito, P. Del Gallo, G. Fornasari, D. Gary, V. Rosetti, A. Vaccari, Effect of silicates on the structure of Ni-containing catalysts obtained from hydrotalcite-type precursors, Catal. Today 128 (2007) 258–263.
[26] J. Pérez-Ramírez, S. Abelló, N.M. vanderPers, Memory effect of activated Mg–Al hydrotalcite: in situ XRD studies during decomposition and gas-phase reconstruction, Chem. Eur. J. 13 (2017) 870–878.
[27] O. Clause, B. Rebours, E. Merlen, F. Trifiró, A. Vaccari, Preparation and characterization of nickel-aluminum mixed oxides obtained by thermal decomposition of hydrotalcite-type precursors, J. Catal. 133 (1992) 231–246.
[28] O. Clause, M. Goncalves Coelho, M. Gazzano, D. Matteuzzi, F. Trifirò, A. Vaccari, Synthesis and thermal reactivity of nickel containing anionic clays, Appl. Clay Sci. 8 (1993) 169–186.
[29] G. Busca, The use of vibrational spectroscopies in studies of heterogeneous catalysis by metal oxides: an introduction, Catal. Today 27 (1996) 323–352.
[30] G.A. Komandin, O.E. Porodinkov, I.E. Spector, A.A. Volkov, Multiphonon absorption in a MgO single crystal in the terahertz range, Phys. Solid State 51 (2009) 2045–2050.
[31] S. Mochizuki, M. Satoh, Infrared spectra of single-crystal NiO at high temperatures, Phys. Stat. Solidi 106 (1981) 667–674.
[32] G. Garbarino, S. Campodonico, A. Romero Perez, M.M. Carnasciali, P. Riani, E. Finocchio, G. Busca, Spectroscopic characterization of Ni/Al_2O_3 catalytic materials for the steam reforming of renewables, Appl. Catal. A: Gen. 452 (2013) 163–173.
[33] P.K. Davies, A. Navrotsky, Thermodynamics of solid solution formation in NiO-MgO and NiO-ZnO, J. Solid State Chem. 38 (1981) 264–276.
[34] A. Chopelas, A.M. Hofmcister, Vibrational spectroscopy of aluminate spinels at 1 atm and of MgAI204 to over 200 kbar, Phys. Chem. Min. 18 (1991) 279–293.
[35] I. Elias, A. Soon, J. Huang, B.S. Haynes, A. Montoya, Atomic order, electronic structure and thermodynamic stability of nickel aluminate, Phys. Chem. Chem. Phys. 21 (2019) 25952–25961.
[36] E.V. Golieva, A.A. Dunaev, A.I. Markova, P.M. Pakhomov, S.D. Khizhnyak, A. E. Chmeld, Infrared reflection and transmission spectra of $MgAl_2O_4$ ceramic spinel, J. Appl. Spectr. 87 (2020) 471–475.
[37] M. Gazzano, W. Kagunya, D. Matteuzzi, A. Vaccari, neutron diffraction studies of polycrystalline Ni/Mg/Al mixed oxides obtained from hydrotalcite-like precursors, J. Phys. Chem. B 101 (1997) 4514–4519.
[38] F. Basile, G. Fornasari, M. Gazzano, A. Vaccari, Rh, Ru and Ir catalysts obtained by HT precursors: effect of the thermal evolution and composition on the material structure and use, J. Mater. Chem. 12 (2002) 3296–3303.
[39] C. Resini, T. Montanari, L. Barattini, G. Ramis, G. Busca, S. Presto, P. Riani, R. Marazza, M. Sisani, F. Marmottini, U. Costantino, Hydrogen production by ethanol steam reforming over Ni catalysts derived from hydrotalcite-like precursors: catalyst characterization, catalytic activity and reaction path, Appl. Catal. A: Gen. 355 (2009) 83–93.
[40] A. Domingo, A. Rodríguez-Fortea, M. Swart, C. de Graaf, R. Broer, Ab initio absorption spectrum of NiO combining molecular dynamics with the embedded cluster approach in a discrete reaction field, Phys. Rev. B 85 (2012), 155143.
[41] G. Leofanti, M. Padovan, G. Tozzola, B. Venturelli, Surface area and pore texture of catalysts, Catal. Today 41 (1998) 207–219.
[42] G. Garbarino, S. Campodonico, A. Romero Perez, M.M. Carnasciali, P. Riani b c, E. Finocchio, G. Busca, Spectroscopic characterization of Ni/Al_2O_3 catalytic materials for the steam reforming of renewables, Appl. Catal. A: Gen. 452 (2013) 163–173.
[43] K.I. Hadjiivanov, G.N. Vayssilov, Characterization of oxide surfaces and zeolites by carbon monoxide as an IR probe molecule, Adv. Catal. 47 (2002) 307–511.
[44] L. Kubelková, J. Nováková, N.I. Jaeger, G. Schulz-Ekloff, Characterization of nickel species at Ni/γ -Al_2O_3 and Ni/faujasite catalysts by carbon monoxide adsorption, Appl. Catal. A: Gen. 95 (1993) 87–101.
[45] S. Derrouiche, D. Bianchi, Heats of adsorption of the linear and bridged CO species on a Ni/Al_2O_3 catalyst by using the AEIR method, Appl. Catal. A: Gen. 313 (2006) 208–217.
[46] V. Sanchez-Escribano, M.A. Larrubia Vargas, E. Finocchio, G. Busca, On the mechanisms and the selectivity determining steps in syngas conversion over supported metal catalysts: an IR study, Appl. Catal. A: Gen. 316 (2007) 68–74.
[47] G. Garbarino, E. Finocchio, A. Lagazzo, I. Valsamakis, P. Riani, V. Sanchez-Escribano, G. Busca, Steam reforming of ethanol–phenol mixture on Ni/Al_2O_3: effect of magnesium and boron on catalytic activity in the presence and absence of sulphur, Appl. Catal. B: Environ. 147 (2014) 813–826.
[48] M.B. Jensen, S. Morandi, F. Prinetto, A. Olafsen Sjåstad, U. Olsbye, G. Ghiotti, FT-IR characterization of supported Ni-catalysts: influence of different supports on the metal phase properties, Catal. Today 197 (2012) 38–49.
[49] G. Garbarino, F. Pugliese, T. Cavattoni, G. Busca, P. Costamagna, A study on CO_2 methanation and steam methane reforming over commercial Ni/calcium aluminate catalysts, Energies 13 (2020) 2792, https://doi.org/10.3390/en13112792.
[50] T. Van Herwijnen, H. Van Doesburg, W.A. De Jong, Kinetics of the methanation of CO and CO_2 on a nickel catalyst, J. Catal. 28 (1973) 391–402.
[51] P. Marocco, E. Alexandru Morosanu, E. Giglio, D. Ferrero, C. Mebrahtu, A. Lanzini, S. Abate, S. Bensaid, S. Perathoner, M. Santarelli, R. Pirone, G. Centi, CO_2 methanation over Ni/Al hydrotalcite-derived catalyst: experimental characterization and kinetic study, Fuel 225 (2018) 230–242.
[52] L.M. Aparicio, Transient isotopic studies and microkinetic modeling of methane reforming over nickel catalysts, J. Catal. 165 (1997) 262–274.
[53] F. Koschany, D. Schlereth, O. Hinrichsen, On the kinetics of the methanation of carbon dioxide on coprecipitated NiAl(O)x, Appl. Catal. B: Environ. 181 (2016) 504–516.
[54] G. Garbarino, D. Belotti, P. Riani, L. Magistri, G. Busca, Methanation of carbon dioxide on Ru/Al_2O_3 and Ni/Al_2O_3 catalysts at atmospheric pressure: catalysts activation, behaviour and stability, Int. J. Hydr. En. 40 (2015) 9171–9182.
[55] G.D. Weatherbee, C.H. Bartolomew, Hydrogenation of CO_2 on group VIII metals: II. Kinetics and mechanism of CO_2 hydrogenation on nickel, J. Catal. 77 (1982) 460–472.
[56] J. Yoshinobu, M. Kawai, Initial adsorption sites of CO on Pt (111) and Ni (100) at low temperature, Surf. Sci. 363 (1996) 105–111.
[57] G. Rupprechter, T. Dellwig, H. Unterhalt, H.-J. Freund, CO adsorption on Ni(100) and Pt(111) studied by infrared–visible sum frequency generation spectroscopy: design and application of an SFG-compatible UHV–high-pressure reaction cell, Top. Catal. 15 (2001) 19–26.
[58] R. Klauser, W. Spieß, A.M. Bradshaw, An IR reflection-absorption study of the CO/Ni(100) adsorption system, J. Electron Spectrosc. Relat. Phenom. 38 (1986) 187.
[59] G. Hincapié, D. López, A. Moreno, Infrared analysis of methanol adsorption on mixed oxides derived from Mg/Al hydrotalcite catalysts for transesterification reactions, Catal. Today 302 (2018) 277–285.